VISUALISING THE FLOWS OF ORTHOGONAL POLYNOMIAL EXPANSIONS OF THE RIEMANN Ξ- FUNCTION

RUDOLPH DWARS, KALPESH MUCHHAL

DECEMBER 19, 2023, VERSION 1.0

Abstract. In a comprehensive paper [1], Dan Romik derives some new infinite series expansions for the Riemann $\Xi(t)$ function in three specific families of orthogonal polynomials; the Hermite polynomials, the symmetric Meixner-Pollaczek polynomials and the continuous Hahn polynomials. We will add the expansion for the Generalised Laguerre polynomials and include a partially successful expansion using the Wilson polynomials. Following Romik, we use the Poisson kernel from the theory of orthogonal polynomials to distort $\Xi(t)$ and thereby induce a 'flow' in its real and complex zeros that obey some dynamical evolution law. In this short paper we aim to visualise these flows that turn out to be quite different for each of the expansions considered.

1. Introduction

The Riemann ξ-function:

$$\xi(s) := \frac{s\,(s-1)}{2}\,\pi^{-s/2}\,\Gamma\left(\frac{s}{2}\right)\,\zeta(s) \tag{1}$$

is an entire function that has been studied extensively. Let $\Xi(t)\colon \mathbb{C} \to \mathbb{C}$ denote the function:

$$\Xi(t) := \xi\left(\frac{1}{2} + it\right), \tag{2}$$

This is an entire even function with functional equations $\Xi(t) = \Xi(-t)$ and $\Xi(\bar{t}) = \overline{\Xi(t)}$, and the Riemann hypothesis is equivalent to the assertion that all the zeroes of $\Xi(t)$ are real. It has the well-known Fourier cosine transform:

$$\Xi(t) := 2\int_0^\infty \Phi(u)\cos(tu)\,du \tag{3}$$

where Φ is the super-exponentially decaying even function:

$$\Phi(u) := 2\sum_{n=1}^{\infty}(2\pi^2 n^4 e^{9u} - 3\pi n^2 e^{5u})\exp(-\pi n^2 e^{4u}). \tag{4}$$

2. Structure of the paper

In the next few chapters we will numerically and visually explore the flows of the zeros of infinite series expansions for $\Xi(t)$ in five specific families of orthogonal polynomials. For comparison's sake, we will start with the Pólya-De Bruijn flow that has been thoroughly explored in the Polymath 15 project [2]. We will derive an additional expansion in terms of the Generalised Laguerre and the Wilson polynomials and conclude the paper with some observations and a short summary.

3. Computations

All computations were done using the advanced FLINT/ARB C-library for arbitrary-precision ball arithmetic [3] supported by random calculations in Maple™[4] to verify the results. Since all flows of real zeros (under RH) eventually culminate into a known non-trivial zero ρ of $\xi(s)$ (i.e. at $\lambda = 0$, or $r = 1$), we used the ordinates of the first few non-trivial zeros as the starting point for tracing their path when λ, r vary. We have used the Newton-Raphson method to locate the zeros at 7 digits accuracy. Our main focus has been on locating the real zeros, however the complex zeros could easily be computed as well.

4. Askey scheme

The Askey scheme is a way of organizing orthogonal polynomials of hypergeometric or basic hypergeometric type into a hierarchy. We use the scheme shown below [5] to illustrate (in green) which orthogonal polynomials have already been successfully applied in the expansion of $\Xi(t)$. To cover all steps of the Askey-ladder, we derived further expansions in terms of the generalised Laguerre and Wilson polynomials (in yellow), the latter with partial success.

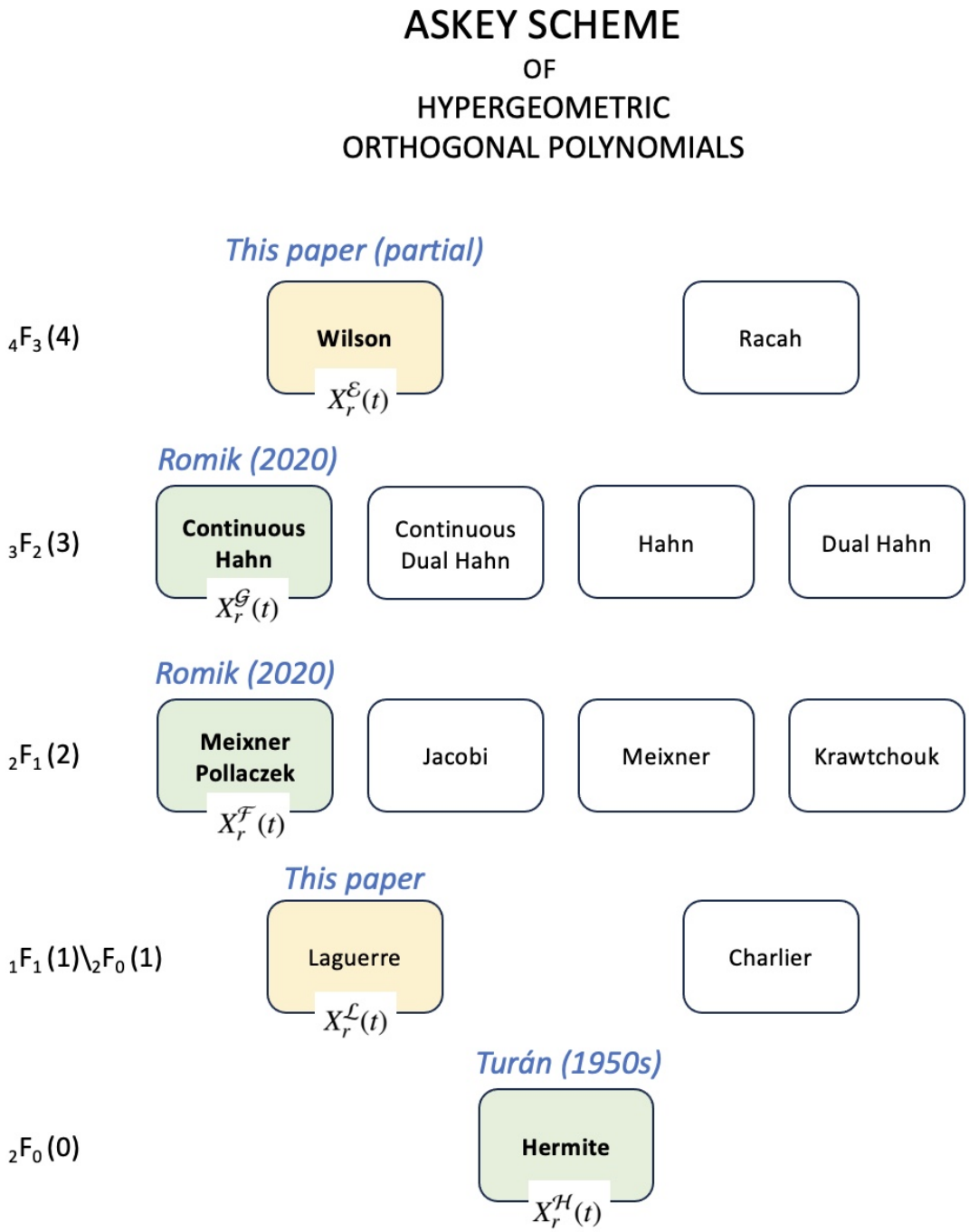

Figure 1. Askey scheme of orthogonal polynomials. Coloured boxes indicate that these polynomials have been successfully applied in expansions of $\Xi(t)$. The label $X_r^{/\mathcal{P}\langle\rangle}(t)$ represents the associated Poisson flow for easy reference.

5. The six flows and how they are evaluated numerically

Our aim is to numerically analyse and visualise the following flows of the real and complex zeros of expansions of $\Xi(t)$. We will follow the notations used in Romik's paper as much as possible. Note that $h_n(t)$ is a HermiteH polynomial and $f_n(t)$, $g_n(t)$, b_n, c_n, d_n are as defined in his paper. The Laguerre coefficient $l_n(\alpha)$ is defined appendix A and the Wilson coefficient e_n in appendix B. The limits of the various infinite series and integrals involved, were chosen such that the required accuracy was achieved.

1. **The Pólya-De Bruijn flow** with parameter $-\infty < \lambda < +\infty, \lambda \in \mathbb{R}$:

$$\Xi_\lambda(t) := 2\int_0^\infty \mathrm{e}^{\lambda x^2}\,\Phi(x)\cos(tx)\,dx \tag{5}$$

Equation and parameters used for the computations are (equation from the Polymath 15 paper [2])

$$\Xi_\lambda(t) := \frac{1}{\sqrt{\pi}}\int_{-8}^{8} \xi\left(\frac{1}{2} + t\,i + 2\sqrt{\lambda}\,x\right)\mathrm{e}^{-x^2}\,dx \tag{6}$$

2. **The Hermite Poisson flow** with parameter $0 < r \le 1, r \in \mathbb{R}$:

$$X_r^{\mathcal{H}}(t) := \sum_{n=0}^{\infty} i^{2n}\,r^{2n}\,b_{2n}\,h_{2n}(t) \tag{7}$$

From Romik's paper we know that this flow can be derived directly from the Pólya-De Bruijn flow:

$$X_r^{\mathcal{H}}(t) := \Xi_{\frac{r^2-1}{4}}(rt) \tag{8}$$

For our computations we simply re-use a scaled version of (6).

3. **The Generalised Laguerre Poisson flow** with parameter $0 < r \le 1, r \in \mathbb{R}$:

In appendix A we derive the expansion of $\Xi(t)$ in terms of the Generalised Laguerre orthogonal polynomials $L_n^\alpha(t)$. For our computations we used these equations and limits:

$$X_r^{\mathcal{L}}(t,\alpha) := \sum_{n=0}^{100} r^n\,l_n(\alpha)\,L_n^\alpha(t) \qquad \alpha > -1 \tag{9}$$

where $l_n(\alpha)$ were pre-computed once for each α chosen as:

$$l_n(\alpha) = \int_{-100}^{100}\left(\frac{iy}{1+iy}\right)^n\left(\frac{1}{1+yi}\right)^{\alpha+1}\Phi(y,60)\,\mathrm{d}y \tag{10}$$

Note 1: The signs of the coefficients $l_n(\alpha)$ appear to fluctuate randomly for all α checked.

4. **The symmetric Meixner-Pollaczek Poisson flow** with parameter $0 < r \le 1, r \in \mathbb{R}$:

$$X_r^{\mathcal{F}}(t) := \sum_{n=0}^{\infty} i^{2n}\,r^{2n}\,c_{2n}\,f_{2n}\left(\frac{t}{2}\right) \tag{11}$$

Equation and parameters used for the computations are:

$$X_r^{\mathcal{F}}(t) := \sum_{n=0}^{100} r^{2n}\,\hat{c}_{2n}\,{}_2F_1\left(-2n, \frac{3}{4}+\frac{it}{2}; \frac{3}{2}; 2\right) \tag{12}$$

where $\hat{c}_n$ were pre-computed once as:

$$\hat{c}_n := (-1)^n\,\frac{\Gamma\left(n+\frac{3}{2}\right)}{\Gamma(n+1)}\,\frac{4\sqrt{2}}{\pi^2}\int_0^{200}\Xi(x)\left|\Gamma\left(\frac{3}{4}+\frac{ix}{2}\right)\right|^2\,{}_2F_1\left(-n, \frac{3}{4}+\frac{ix}{2}; \frac{3}{2}; 2\right)dx \tag{13}$$

5. **The continuous Hahn Poisson flow** with parameter $0 < r \leq 1, r \in \mathbb{R}$:

$$X_r^{\mathcal{G}}(t) \coloneqq \sum_{n=0}^{\infty} i^{2n}\, r^{2n}\, d_{2n}\, g_{2n}\left(\frac{t}{2}\right) \tag{14}$$

Equation and parameters used for the computations are:

$$X_r^{\mathcal{G}}(t) \coloneqq \sum_{n=0}^{100} r^{2n}\, \hat{d}_{2n}\, {}_3F_2\left(-2n, 2n+2, \frac{3}{4}+\frac{it}{2}; \frac{3}{2}, \frac{3}{2}; 1\right) \tag{15}$$

where $\hat{d}_n$ were pre-computed once as:

$$\hat{d}_n \coloneqq (-1)^n\, (n+1)^2\, \frac{16}{\pi^3} \int_0^{200} \Xi(x) \left|\Gamma\left(\frac{3}{4}+\frac{ix}{2}\right)\right|^4\, {}_3F_2\left(-n, n+2, \frac{3}{4}+\frac{ix}{2}; \frac{3}{2}, \frac{3}{2}; 1\right) dx \tag{16}$$

6. **The Wilson Poisson flow** with parameter $0 < r \leq 1, r \in \mathbb{R}$:

In appendix B we share our attempt to derive an expansion of $\Xi(t)$ in terms of the Wilson orthogonal polynomials. However, we were only partially successful and start to wonder whether such an direct expansion actually exists. We did find a way to expand $\Xi(t)$, but now with the Poisson flow of $\frac{\Xi(t)-\Xi(0)}{t^2}$. This function also has some interesting properties and we therefore included its visualised flow.

The computations were done using the following limits:

$$X_r^{\mathcal{E}}(t) \coloneqq \Xi(0) - t^2 \sum_{n=0}^{200} r^n\, e_n\, {}_4F_3\left(-n, n+2, \frac{1}{2}+\frac{it}{4}, \frac{1}{2}-\frac{it}{4}; \frac{3}{2}, 1, \frac{3}{2}; 1\right) \tag{17}$$

where e_n were pre-computed once as:

$$e_n \coloneqq \int_0^{200} \Phi(u)\, \tanh^{2n+2}(u)\, \mathrm{d}u \tag{18}$$

Note 1: all e_n are positive. We did not explore a possible asymptotic formula.

Note 2: Even though this expansion in terms of Wilson polynomials works well numerically, its structure deviates from the previous ones. For instance, the e_n terms for odd n are not equal to zero and the $(-1)^n$ factor is missing (although the latter could easily be recovered from the $\tanh^{2n+2}(u)$ factor).

Note 3: The RH would follow when (for $r = 1$) only real t solutions exist of:

$$t^2 \sum_{n=0}^{\infty} e_n\, {}_4F_3\left(-n, n+2, \frac{1}{2}+\frac{it}{4}, \frac{1}{2}-\frac{it}{4}; \frac{3}{2}, 1, \frac{3}{2}; 1\right) = \Xi(0) \tag{19}$$

An infinite number of solutions for t real must exist, however for solutions for t complex (i.e. zeros off the critical line) things are much more complicated. The factor t^2 will always be complex for $t = a+bi, a, b \neq 0$, hence the factor $\sum_{n=0}^{\infty} e_n\, {}_4F_3\left(-n, n+2, \frac{1}{2}+\frac{it}{4}, \frac{1}{2}-\frac{it}{4}; \frac{3}{2}, 1, \frac{3}{2}; 1\right)$ must be the exact conjugate of t^2 to become real and equal to $\Xi(0)$. The existence of such exact conjugate is equivalent to the RH and obviously very hard to prove.

6. Visualization of the Pólya-De Bruijn flow

The graph below visualises the trajectories of the real zeros and the collision points at a certain λ where they become complex.

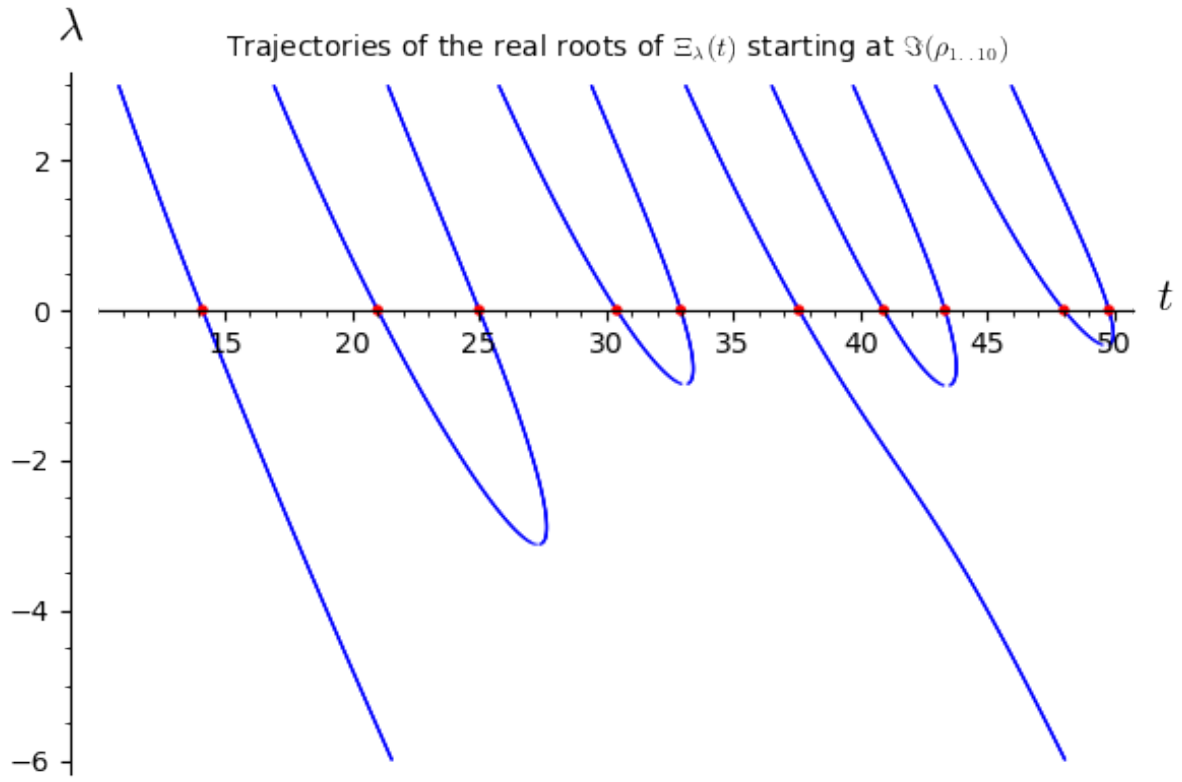

Figure 2. Each blue dot represents a real root of $\Xi_\lambda(t)$. These jointly constitute the blue "trajectories" when λ is varied. Some collisions occur when $\lambda < 0$ where the zeros become complex. The ordinates of the non-trivial zeros of $\xi(s)$ are shown as red dots. The concept of "hyperbolicity", i.e. the preservation of the reality of the zeros when λ become more positive, is clearly visible in the flows.

Some facts proven in the Polymath 15 project:

- In 2018 Tao and Rodgers [6] proved Newman's lower bound conjecture that $\lambda \geq 0$, They used techniques from Random Matrix theory to predict the 'time to cool down' and compared this to known facts about the distribution of zeros at $\lambda = 0$. A student of Tao, Alex Dobner later found a much simpler proof [7] that $\lambda \geq 0$ which avoids the heat equation approach. Dobner's approach instead relies on a Riemann-Siegel type approximation for $\Xi_\lambda(t)$ in order to demonstrate the existence of zeros off the critical line.
- After further numerical verification of the RH by Platt et al [8], it has now been proven that the upper bound of the De Bruijn-Newman constant is $\lambda \leq 0.2$. Hence, a breach of the RH would imply that there exists some pair complex zeros that collide in the region $0 \leq \Xi_\lambda(t) \leq 0.2$.
- For increasingly positive λ we know that the trajectories of zeros converge to a deterministic arithmetic progression.
- Increasingly negative λ will induce more pairs of complex zeros that eventually will organise themselves on deterministic curves. A sparse, but regular set of real zeros remains real 'forever' (probably because they are too far apart to be able to collide).

7. Visualization of the Hermite Poisson flow

The graph below visualises the parallel trajectories of the real zeros. There don't appear to be any collision points at a certain r where they become complex. We have extended our computations for some $r > 1$ and observed the distribution of the zeros doesn't change much.

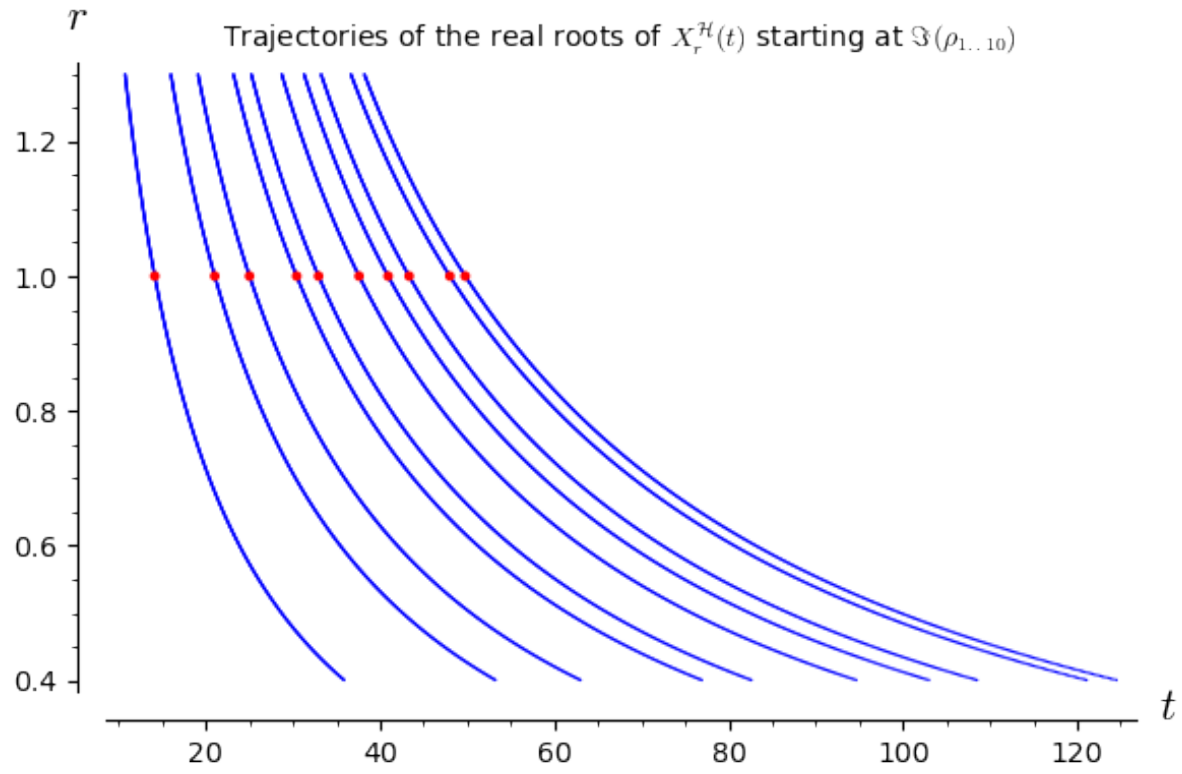

Figure 3. Each blue dot represents a real root of $X_r^{\mathcal{H}}(t)$. These jointly constitute the blue "trajectories" when r is varied. The ordinates of the non-trivial zeros of $\xi(s)$ are shown as red dots. Data has been computed from $r = 0.001...1$ in steps of 0.001 and from 1..1.3 in steps of 0.001. For better visibility only $r \geq 0.4$ is shown.

Some observations:

- After analysing the direct link with the Pólya-De Bruijn flow $X_r^{\mathcal{H}}(t) := \Xi_{\frac{r^2-1}{4}}(rt)$ a bit further, we see that when r varies between 0 and 1 the associated λ varies from $-0.25, ..., 0$. However, the Ξ function is scaled by rt simultaneously and it is difficult to predict what sort of pattern this induces.

- Since both flows are equivalent, also in terms of the dynamics of the zeros, we would expect collisions to occur at some point. Note from figure 2 that collisions amongst the first 10 zeros don't occur yet when λ only varies between $-0.25, ..., 0$.

- The scaling of t in $\Xi(rt)$ will become more dominant the closer r gets to 0. We are not sure whether or not collisions will occur in this domain since the trajectories of the zeros become increasingly close and computations start to interfere.

8. Visualization of the Generalised Laguerre Poisson flow

The graph below visualises the trajectories of the real zeros. They clearly mimic the pattern and collision points of the Pólya-De Bruijn flow. We have extended our computations into the domain $r > 1$ and observed the distribution of the zeros also here converges towards an arithmetic progression.

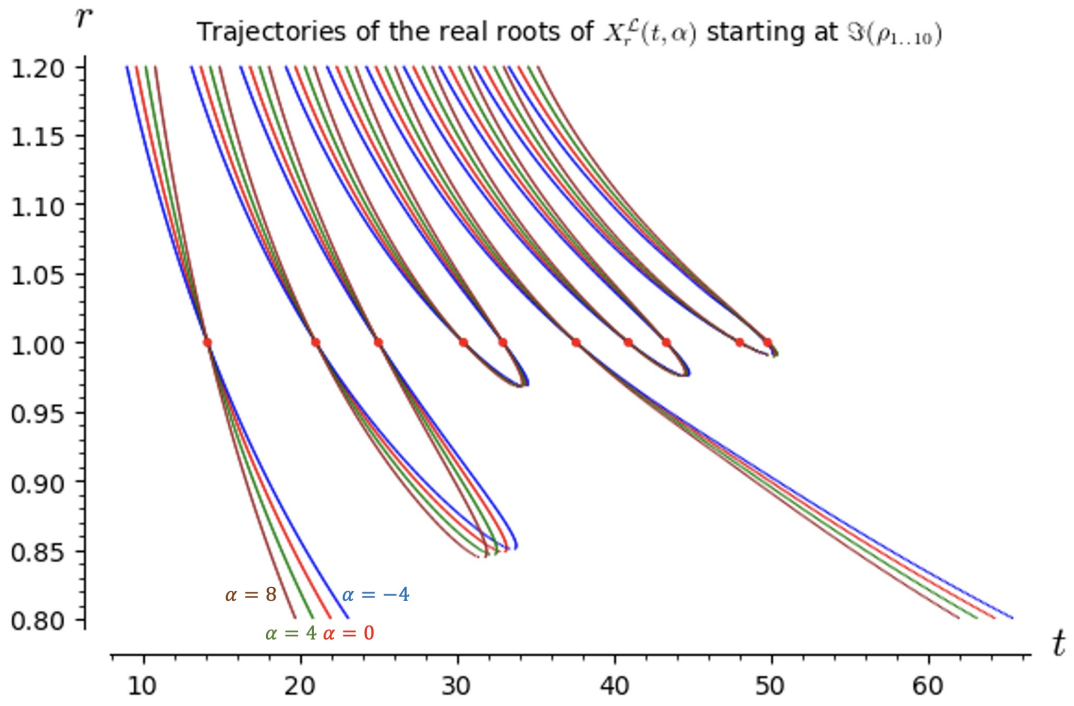

Figure 4. Each coloured dot represents a real root of $X_r^{\mathcal{L}}(t,\alpha)$. These jointly constitute the "trajectories" when r is varied. We show the trajectories for $X_r^{\mathcal{L}}(t,-4), X_r^{\mathcal{L}}(t,0), X_r^{\mathcal{L}}(t,4), X_r^{\mathcal{L}}(t,8)$ in respectively blue, red, green and brown. The ordinates of the non-trivial zeros of $\xi(s)$ are shown as red dots at $r = 1$. Data has been computed from $r = 0.001...1$ in steps of 0.001 and from 1..1.2 in steps of 0.001. For better visibility only $r \geq 0.8$ is shown. The concept of "hyperbolicity" is clearly visible.

Some observations:

- The similarity of the patterns with the Pólya-De Bruijn flow is striking. We would expect these flows to be connected somehow in a similar fashion as the Hermite flow, however after some attempts we found this proves to be difficult to make explicit (even for $\alpha = \pm\frac{1}{2}$).
- An increase of $\alpha > 0$ appears to induce a clockwise rotation of the real roots of $X_r^{\mathcal{L}}(t,0)$ around $r = 1$. This implies the collision points in the domain $r < 1$ occur at lower r when α increases. When we have a collision happening in the domain $r > 1$ (i.e. a failure of the RH), this rotation would move that collision to a later point (i.e. higher r) when α increases.
- A decrease of $\alpha < 0$ appears to induce an anti-clockwise rotation of the real roots of $X_r^{\mathcal{L}}(t,0)$ around $r = 1$. This implies the collision points in the domain $r < 1$ occur at higher r when α decreases. When we have a collision happening in the domain $r > 1$ (i.e. a failure of the RH), this rotation would move that collision to an earlier point (i.e. lower r) when α decreases.
- Is there anything else that could be derived from this rotation induced by α? Is there maybe some law that dictates that these rotation points have to be real? It is known that when α is non-negative, then L_n^{α} has n real, strictly positive roots which all reside in the interval:

$$\left(0, n + \alpha + (n-1)\sqrt{n+\alpha}\right]$$

.

9. Visualization of the symmetric Meixner-Pollaczek Poisson flow

The graph below visualises the trajectories of the real zeros and the collision points at a certain positive r where they become complex. We extended our computations for some $r > 1$ (acknowledging that this might violate the domain constraints of the Poisson kernel) and included a few more non-trivial zeros to better visualise the emerging patterns.

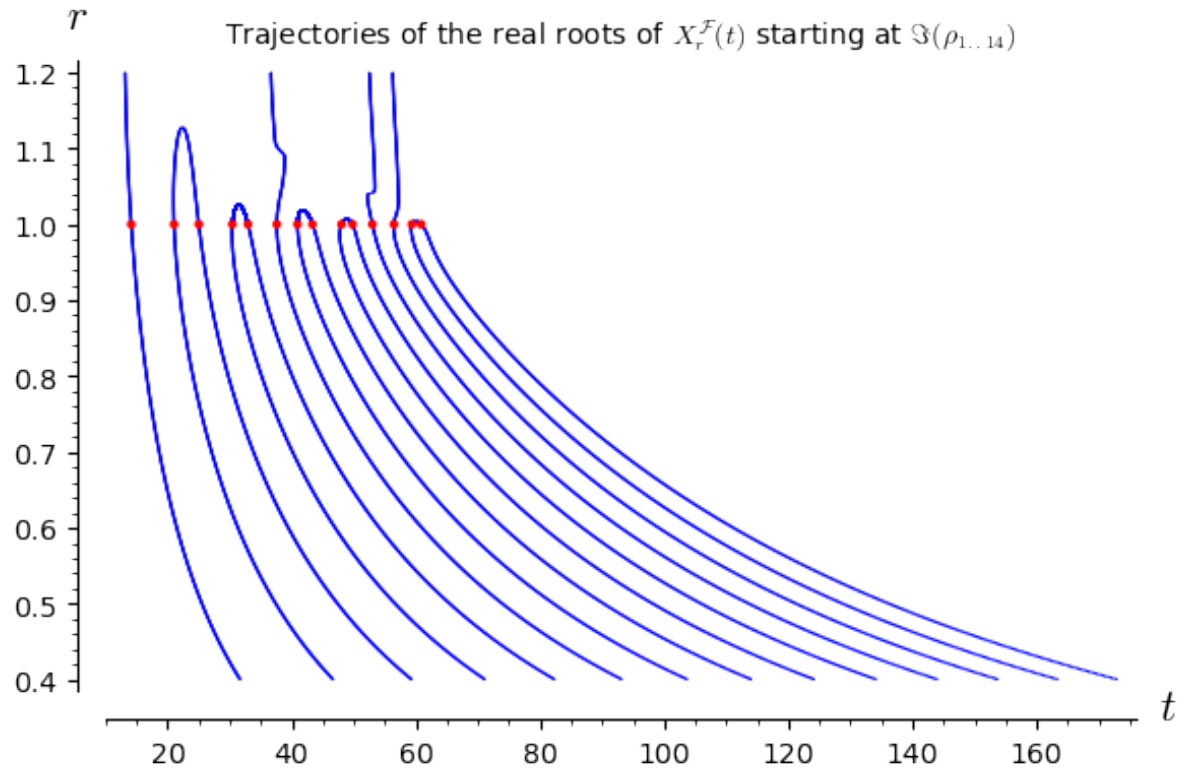

Figure 5. Each blue dot represents a real root of $X_r^{\mathcal{F}}(t)$. These jointly constitute the blue "trajectories" when r is varied. The ordinates of the non-trivial zeros of $\xi(s)$ are shown as red dots. Data has been computed from $r = 0.001...1$ in steps of 0.001. For better visibility only $r \geq 0.4$ is shown. Distribution complexity increases when $r \to 1$.

Some observations:

- The distribution of the real zeros at $r = 1$ appears to converge towards some arithmetic progression when r is varied towards 0.
- The complexity of the distribution clearly increases for $r \to 1$, since the trajectories become increasingly influenced by the primes in the Euler product forcing them to land on the right spot. This flow is clearly different from the previous Poisson flows.
- After extending the computations into the $r > 1$ domain, some collisions became visible close to $r = 1$ and some real trajectories appear to stay real 'forever' (checked up to $r = 30$, although this might violate the domain of the Poisson kernel).
- A failure of the RH would occur when a collision between two real zeros happens somewhere in the domain $r < 1$. Or put simpler: the RH implies no complex zeros exist for any $r \leq 1$. It is almost the "vertically flipped" version of the Pólya-De Bruijn flow.

10. Visualization of the continuous Hahn Poisson flow

The graph below visualises the trajectories of the real zeros and the collision points at a certain increasingly small positive and negative r where they become complex. We extended our computations for some $r > 1$ (acknowledging that this might violate the domain constraints of the Poisson kernel) to better visualise the emerging oscillations.

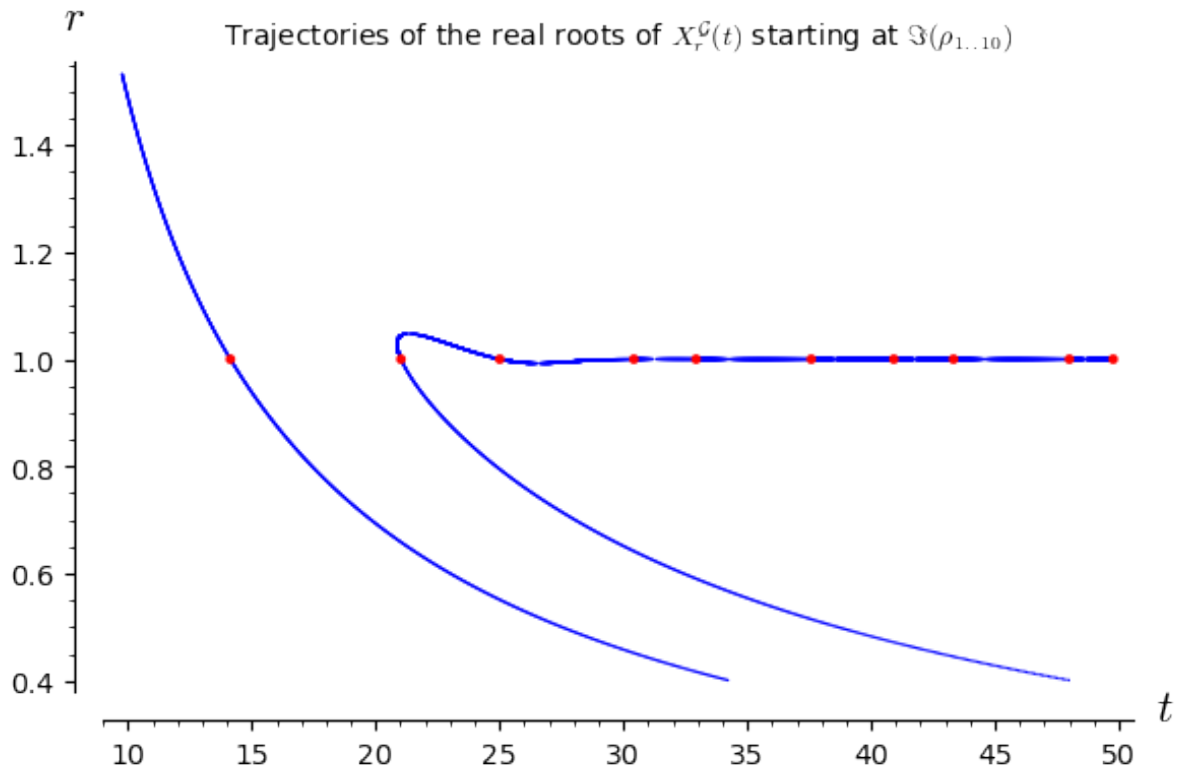

Figure 6. Each blue dot represents a real root of $X_r^{\mathcal{G}}(t)$. These jointly constitute the blue "trajectories" when r is varied. The ordinates of the non-trivial zeros of $\xi(s)$ are shown as red dots. Based on the initial pattern observed, data was also computed for $r > 1$. For higher t, step sizes of r had to be reduced to be able to locate the real zeros. For visibility only $0.4 \leq r \leq 1.5$ is shown.

Some observations:

- The flow of the zeros in this expansion is fundamentally different from the previous ones. After computing the real zeros up till $r = 1$, the lower halves of an oscillating pattern around the line $r = 1$ emerged. When computing the zeros $r > 1$, the top halves of the oscillations appeared. The amplitude of the oscillations rapidly decreases and we had to use increasingly smaller step sizes to find the zeros. This once again shows how incredibly sensitive the $\Xi(t)$ function is to distortions and once again supports Newman's observation that "if the RH is true, then it is barely so."
- The first two zeros form an exception and seem to collide and become complex at some very low r and high t, the exact location (if not infinity) is difficult to compute (see Figure 8).
- A failure of the RH would occur when there exists a local minimum ($r > 1$) or local maximum ($r < 1$) in the oscillations between two subsequent real non-trivial zeros (see Figure 10).

Zooming in a bit on the oscillations gives:

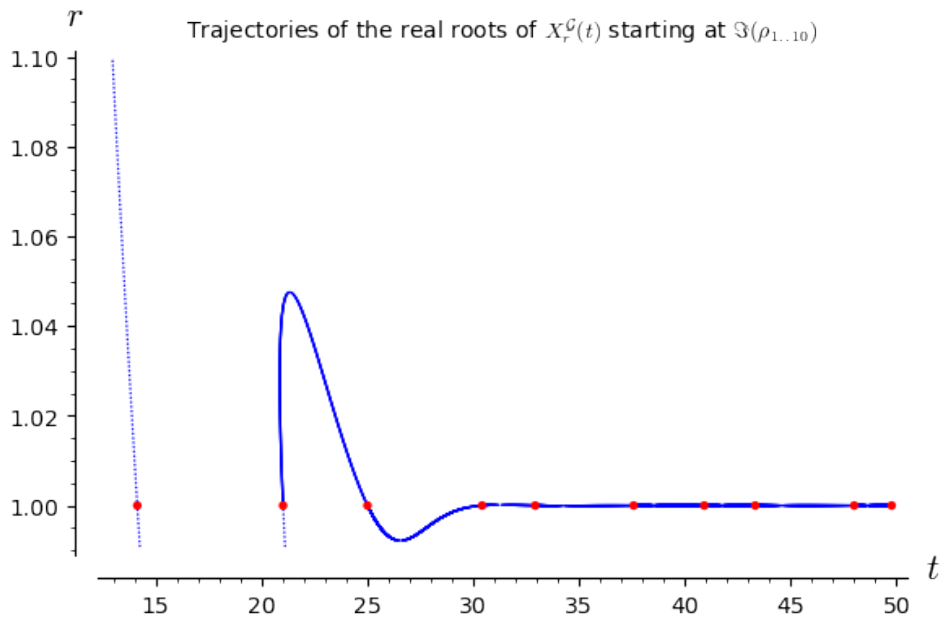

FIGURE 7. Each blue dot represents a real root of $X_r^{\mathcal{G}}(t)$. These jointly constitute the blue "trajectories" when r is varied. The ordinates of the non-trivial zeros of $\xi(s)$ are shown as red dots. For better visibility only $0.99 \leq r \leq 1.1$ is shown.

Zooming out a bit yields:

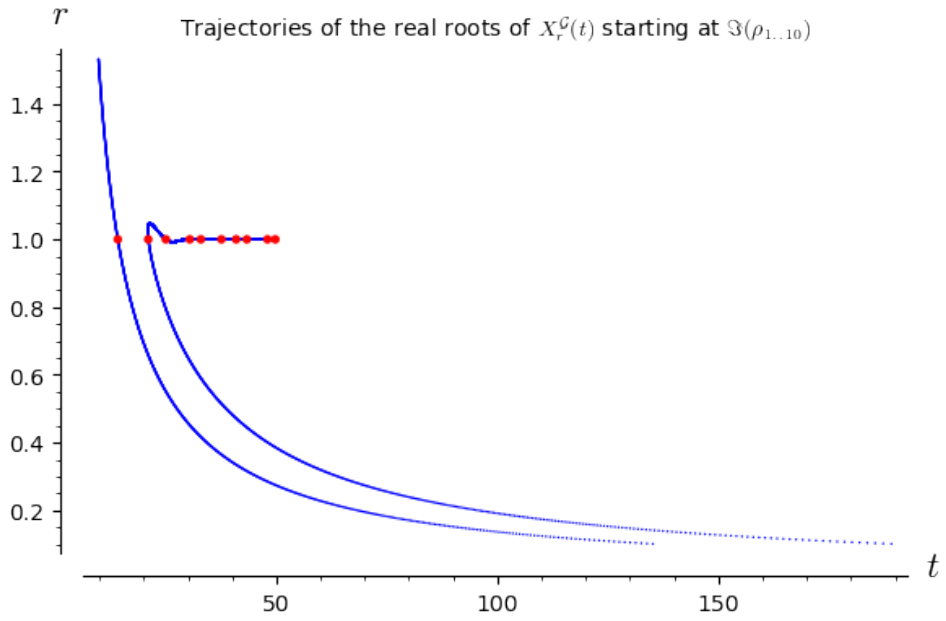

FIGURE 8. Each blue dot represents a real root of $X_r^{\mathcal{G}}(t)$. These jointly constitute the blue "trajectories" when r is varied. The ordinates of the non-trivial zeros of $\xi(s)$ are shown as red dots. For better visibility only $0.1 \leq r \leq 1.5$ is shown.

11. Visualization of the Wilson Poisson flow

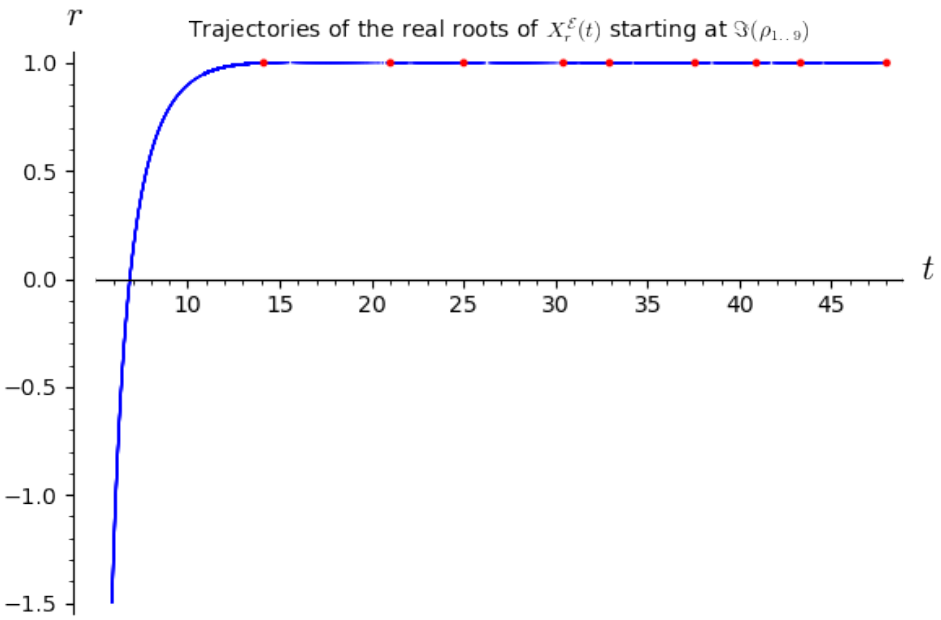

Figure 9. Each blue dot represents a real root of $X_r^{\mathcal{E}}(t)$. These jointly constitute the blue "trajectories" when r is varied. The ordinates of the non-trivial zeros of $\xi(s)$ are shown as red dots. For better visibility only $r > -1.5$ is shown. The trajectory crosses the line $r = 0$ when $\Xi(0) - t^2\, e_0 = 0$, which occurs at $t = \pm 6.848902562$

.

Some observations:

- The flow of the zeros in this expansion is similar to the previous one, however lacks the anomaly between ρ_1 and ρ_2. This one therefore feels a bit more "natural". We again see an oscillating pattern around the line $r = 1$. The amplitude of the oscillations again rapidly decreases and we had to use increasingly smaller step sizes to find the real zeros.
- A failure of the RH would occur when there exists a local minimum ($r > 1$) or local maximum ($r < 1$) in the oscillations between two subsequent real non-trivial zeros (see Figure 10).

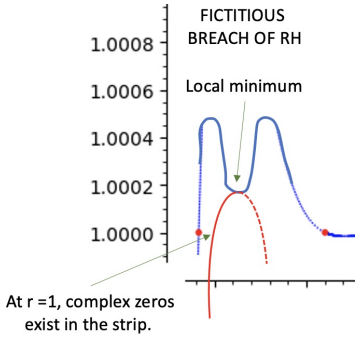

Figure 10. This graph illustrates a fictitious failure of the RH due to the existence of a local minimum in the trajectory of the real zeros (blue). This induces an extra collision at some $r > 1$ located between two subsequent real zeros and generates a pair of complex zeros (red). When r is reduced further, these complex zeros will enter the critical strip at $r = 1$ and violate the RH. For a local maximum failure, the situation is just mirrored.

Zooming in a bit yields:

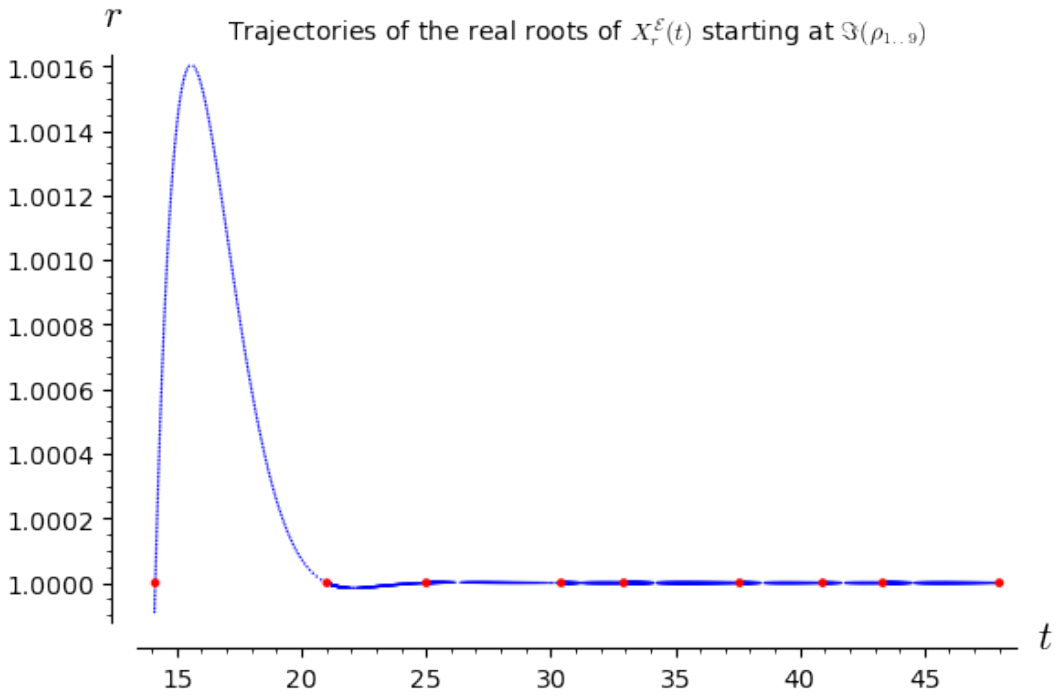

FIGURE 11. Each blue dot represents a real root of $X_r^{\mathcal{E}}(t)$. These jointly constitute the blue "trajectories" when r is varied. The ordinates of the non-trivial zeros of $\xi(s)$ are shown as red dots. For better visibility only $r > 0.9999$ is shown.

12. CONCLUDING REMARKS

Based on the analysis and observations about the visuals we conclude:

- The continuous Hahn and Wilson flows are quite intriguing since they show an oscillating pattern in the trajectory of the real zeros with an amplitude that rapidly decreases. Their behaviour bears some similarities to the flow we observed when distorting $\Xi(t)$ by a fractional integration/differentiation operator α around $\alpha = 0$. This flow has been explored in this (not yet published) paper [9].

- The common characteristic of all flows is that they start off with a distortion of the original function $\Xi(t)$ at $r = 1$. We indeed observe that all information flows from this origin and might help explain what happens in the 'distorted' domain ($r \neq 1$). Unfortunately, there is no information (as yet) gained from the 'distorted' domain that tells us more about its origin at $r = 1$.

- However, we find it really encouraging to see that the visualised flows for each orthogonal polynomial expansion are quite different from each other. This induces new hope that there could exist a yet undiscovered expansion that induces a flow that does provide new information about the reality of the zeros at $r = 1$. Such a result might follow from a more deterministic differential equation that underpins the dynamical evolution of the real zeros. For instance, for the oscillations in the continuous Hahn flow, the RH would follow when a proof existed that between two real zeros, the trajectories of real zeros can never decline when $r > 1$ and never incline when $r < 1$ (thereby ruling out the existence of local minima and maxima).

13. Summary and references

Hypergeom complexity	Orthogonal polynomial	Poisson flow	Expansion $\Xi(t)$	Key observations about the visualized flow.
${}_4F_3(4)$	Wilson	$X_r^{\mathcal{E}}(t)$	?	The trajectories of the real zeros smoothly oscillate increasingly close around the line r=1.
${}_3F_2(3)$	Continuous Hahn	$X_r^{\mathcal{G}}(t)$	✓	The trajectories of the real zeros oscillate around the line r=1 with an exception between ρ_1 and ρ_2.
${}_2F_1(2)$	Meixner Pollaczek	$X_r^{\mathcal{F}}(t)$	✓	The trajectories of the real zeros converge towards an arithmetic progression when r goes to 0.
${}_1F_1(1)$	Generalised Laguerre	$X_r^{\mathcal{L}}(t,\alpha)$	✓	The trajectories of the real zeros rotate clockwise around r=1 when α >0 in L_n^{α} and vice versa for α <0.
${}_2F_0(0)$	Hermite	$X_r^{\mathcal{H}}(t)$	✓	The trajectories of the real zeros seem parallel, however should be equivalent to Pólya-De Bruijn flow.

Figure 12. Overview of the key observations

References

[1] Romik, D. *Orthogonal polynomial expansions for the Riemann xi function in the Hermite, Meixner-Pollaczek, and continuous Hahn bases.*, Acta Arithmetica 200 (2021), 259-329. Note: this paper exists in two different versions with different titles. See this page: https://www.math.ucdavis.edu/ romik/riemannxi/ for additional information and related resources.

[2] D. H. J. Polymath, *Effective approximation of heat flow evolution of the Riemann ξ function, and a new upper bound for the de Bruijn-Newman constant*, Polymath 15 project, https://arxiv.org/abs/1904.12438,

[3] Johansson, F. et al, *FLINT/Arb - a C library for arbitrary-precision ball arithmetic*, https://flintlib.org.

[4] Maplesoft, *Mathematics-based software solutions*, https://www.maplesoft.com.

[5] Koekoek, R. and Swarttouw, R. F., *The Askey-Scheme of Hypergeometric Orthogonal Polynomials and its q-Analogue*, Delft, Netherlands: Technische Universiteit Delft, Faculty of Technical Mathematics and Informatics Report 98-17, 1-168, 1998.

[6] B. Rodgers and T. Tao. *The De Bruijn-Newman constant is non-negative.*, ArXiv e-prints, 2018. https://arxiv.org/abs/1801.05914

[7] Dobner, A, *A proof of Newman's Conjecture for the extended Selberg class*, Acta Arithmetica 201 (2021), https://arxiv.org/abs/2005.05142

[8] Platt, D., Trudgian, T., *The Riemann hypothesis is true up to* $3\,10^{12}$, Bulletin of the London Mathematical Society, Volume 53, Issue 3, Pages: 643-962, June 2021

[9] Muchhal, K., Dwars, R., *Fractional integrals and derivatives of the Riemann ξ-function*, Version draft, available on , `https://drive.google.com/file/d/1B-h1hbUcsgkiS8T05N1gCiAJLdtuY-Uh/view?usp=share_link`, December 2023

[10] Wilson, James A., *Some hypergeometric orthogonal polynomials*, SIAM Journal on Mathematical Analysis p690–701, 1980

Appendices

Appendix A. Derivation of an expansion of $\Xi(t)$ in terms of Generalised Laguerre polynomials

The Generalised orthogonal Laguerre polynomials are defined by the hypergeometric function:

$$L_n^\alpha(x) \coloneqq \frac{\Gamma(\alpha+1+n)}{\Gamma(\alpha+1)\,\Gamma(n+1)}\, M(-n,\alpha+1,x) \tag{20}$$

where $M(a,b,c)$ is the confluent KummerM function. A few of the main properties of these polynomials we will need are listed below (see appendix A of [1]):

Weight:

$$we(x,\alpha) = \mathrm{e}^{-x}\, x^\alpha \tag{21}$$

Orthogonality relation:

$$\int_{-\infty}^{\infty} L_m^\alpha(x)\, L_n^\alpha(x)\, we(x,\alpha)\mathrm{d}x = \delta_{m,n}\frac{\Gamma(\alpha+1+n)}{\Gamma(n+1)} \quad \text{when } m = n \text{ and 0 otherwise.} \tag{22}$$

Generating function for $|z| < 1$:

$$\sum_{n=0}^{\infty} L_n^\alpha(x)\, z^n = \frac{1}{(1-z)^{\alpha+1}}\, \exp\left(-\frac{xz}{1-z}\right) \tag{23}$$

After mapping $z \mapsto \frac{iy}{1+iy}$, this reduces to:

$$\sum_{n=0}^{\infty} L_n^\alpha(x) \left(\frac{iy}{1+iy}\right)^n = \mathrm{e}^{-ixy} \left(\frac{1}{1+yi}\right)^{-\alpha-1} \tag{24}$$

Our target integral representation of $\Xi(t)$ is:

$$\Xi(t) \coloneqq \int_{-\infty}^{\infty} \mathrm{e}^{-itx}\, \Phi(x)\, \mathrm{d}x \tag{25}$$

where $\Phi(x)$ is defined in equation (4). After applying a correction term, substituting the generating function and swapping the sum and integral, we obtain:

$$\Xi(t) \coloneqq \sum_{n=0}^{\infty} L_n^\alpha(t) \int_{-\infty}^{\infty} \left(\frac{iy}{1+iy}\right)^n \left(\frac{1}{1+yi}\right)^{\alpha+1} \Phi(y)\, \mathrm{d}y \tag{26}$$

The Poisson flow becomes:

$$X_r^{\mathcal{L}}(t,\alpha) \coloneqq \sum_{n=0}^{\infty} r^n\, L_n^\alpha(t)\, l_n(\alpha) \tag{27}$$

$$l_n(\alpha) = \int_{-\infty}^{\infty} \left(\frac{iy}{1+iy}\right)^n \left(\frac{1}{1+yi}\right)^{\alpha+1} \Phi(y)\, \mathrm{d}y \tag{28}$$

or equivalently, but only valid for $\alpha > -1$:

$$l_n(\alpha) = \frac{1}{\Gamma(\alpha+1)} \int_{0^+}^{\infty} \Xi(y)\, y^\alpha\, M(\alpha+1+n,\alpha+1,-y)\, \mathrm{d}y \tag{29}$$

Note 1: All equations above have been verified numerically, however a more rigorous proof about the domain of convergence would be desired.

Appendix B. Derivation of an expansion of $\Xi(t)$ in terms of orthogonal Wilson polynomials

In 1980, Wilson [10] introduced a family of orthogonal polynomials defined by the hypergeometric function:

$$W_n(y^2;a,b,c,d) := (a+b)_n(a+c)_n(a+d)_n\,{}_4F_3(-n,n+a+b+c+d-1,a+iy,a-iy;a+b,a+c,a+d;1) \tag{30}$$

where $(a)_n$ is the Pochhammer symbol. A few of the main properties of these polynomials we will need are listed below [5]:

Weight:

$$we(x) = \left|\frac{\Gamma(a+ix)\,\Gamma(b+ix)\,\Gamma(c+ix)\;\Gamma(d+ix)}{\Gamma(2ix)}\right|^2 \tag{31}$$

Orthogonality relation:

$$\int_0^\infty W_m(x^2;a,b,c,d)\,W_n(x^2;a,b,c,d)\,we(x)\mathrm{d}x = \delta_{m,n}M(n) \quad \text{when } m=n \text{ and 0 otherwise.} \tag{32}$$

with:

(33)

$$M(n) = 2\pi n!(a+b+c+d+n-1)_n\frac{\Gamma(a+b+n)\Gamma(a+c+n)\Gamma(a+d+n)\Gamma(b+c+n)\Gamma(b+d+n)\Gamma(c+d+n)}{\Gamma(a+b+c+d+2n)}$$

Generating function for $|z|<1$:

$$\sum_{n=0}^\infty \frac{W_n(y^2;a,b,c,d)}{(a+d)_n(b+c)_n\,n!}\,z^n = {}_2F_1\,(a+iy,d+iy,a+d;z)\;{}_2F_1\,(b-iy,c-iy,b+c;z) \tag{34}$$

We now set: $y=t/4, a=1/2, b=1, c=1/2, d=1$ and obtain:

$$W_n\left(\left(\frac{t}{4}\right)^2;\frac{1}{2},1,\frac{1}{2},1\right) = \left(\frac{3}{2}\right)_n\left(\frac{3}{2}\right)_n n!\,{}_4F_3\left(-n,n+2,\frac{1}{2}+\frac{it}{4},\frac{1}{2}-\frac{i\,t}{4};\frac{3}{2},1,\frac{3}{2};1\right) \tag{35}$$

whose generating function for $|z|<1$ becomes:

$$\sum_{n=0}^\infty \frac{W_n\left(\left(\frac{t}{4}\right)^2;\frac{1}{2},1,\frac{1}{2},1\right)}{\left(\frac{3}{2}\right)_n\left(\frac{3}{2}\right)_n n!}\,z^n = {}_2F_1\left(\frac{1}{2}+\frac{it}{4},1+\frac{it}{4},\frac{3}{2};z\right){}_2F_1\left(\frac{1}{2}-\frac{it}{4},1-\frac{it}{4},\frac{3}{2};z\right) \tag{36}$$

After mapping $z\mapsto\frac{(1-x)^2}{(1+x)^2}$, this nicely reduces (on both sides) to:

$$\sum_{n=0}^\infty {}_4F_3\left(-n,n+2,\frac{1}{2}+\frac{it}{4},\frac{1}{2}-\frac{i\,t}{4};\frac{3}{2},1,\frac{3}{2};1\right)\left(\frac{(1-x)^2}{(1+x)^2}\right)^n = -\frac{\left(-2+x^{-\frac{it}{2}}+x^{\frac{it}{2}}\right)(1+x)^2}{t^2\,(1-x)^2} \tag{37}$$

which is valid for $x\in\mathbb{R}^+, t\in\mathbb{C}$. Our target integral representation of $\Xi(t)$ is:

$$\Xi(t) := \int_{0^+}^\infty w(x)\,x^{-\frac{3}{4}+\frac{it}{2}}\mathrm{d}x \tag{38}$$

with:

$$w(x) := \sum_{n=1}^\infty\left(2\,\pi^2\,n^4\,x^2-3\,\pi\,n^2\,x\right)\mathrm{e}^{-\pi\,n^2\,x} \tag{39}$$

Using $\Xi(t) = \Xi(-t)$, we only need a few correction terms to obtain the target integral:

$$\Xi(t) := \frac{1}{2}\int_{0^+}^{\infty} \frac{\left(-2 + x^{-\frac{it}{2}} + x^{\frac{it}{2}}\right)(1+x)^2}{t^2\,(1-x)^2}\, w(x)\, x^{-\frac{3}{4}}\, \frac{t^2\,(1-x)^2}{(1+x)^2} + 2w(x)\, x^{-\frac{3}{4}}\,\mathrm{d}x \tag{40}$$

which simplifies into:

$$\Xi(t) := \Xi(0) + \frac{t^2}{2}\int_{0^+}^{\infty} \frac{\left(-2 + x^{-\frac{it}{2}} + x^{\frac{it}{2}}\right)(1+x)^2}{t^2\,(1-x)^2}\, w(x)\, x^{-\frac{3}{4}}\, \frac{(1-x)^2}{(1+x)^2}\mathrm{d}x \tag{41}$$

Substituting the generating function and swapping the integral and sum yields:

$$\Xi(t) := \Xi(0) - \frac{t^2}{2}\sum_{n=0}^{\infty} {}_4F_3\left(-n, n+2, \frac{1}{2}+\frac{it}{4}, \frac{1}{2}-\frac{it}{4}; \frac{3}{2}, 1, \frac{3}{2}; 1\right)\int_{0^+}^{\infty} w(x)\, x^{-\frac{3}{4}}\left(\frac{1-x}{1+x}\right)^{2n+2}\mathrm{d}x \tag{42}$$

After the variable change $x = \mathrm{e}^{2u}$ we reach:

$$\Xi(t) := \Xi(0) - t^2\sum_{n=0}^{\infty} {}_4F_3\left(-n, n+2, \frac{1}{2}+\frac{it}{4}, \frac{1}{2}-\frac{it}{4}; \frac{3}{2}, 1, \frac{3}{2}; 1\right)\int_{0}^{\infty} \Phi(u)\, \tanh^{2n+2}(u)\,\mathrm{d}u \tag{43}$$

where $\Phi(u)$ is defined in (4).

The target Poisson Kernel is:

$$p_r^{\mathcal{E}}(x,y) = \frac{2}{\pi^3}\sum_{n=0}^{\infty}(n+1)\, {}_4F_3\left(-n, n+2, \frac{1}{2}+\frac{ix}{4}, \frac{1}{2}-\frac{ix}{4}; \frac{3}{2}, 1, \frac{3}{2}; 1\right){}_4F_3\left(-n, n+2, \frac{1}{2}+\frac{iy}{4}, \frac{1}{2}-\frac{iy}{4}; \frac{3}{2}, 1, \frac{3}{2}; 1\right) r^n \tag{44}$$

and in line with the theory, this correctly yields the equation:

$$\int_{-\infty}^{\infty} p_r^{\mathcal{E}}(x,y)\, W_n\left(\left(\frac{y}{4}\right)^2; \frac{1}{2}, 1, \frac{1}{2}, 1\right) we\left(\frac{y}{4}\right)\mathrm{d}y = r^n\, W_n\left(\left(\frac{x}{4}\right)^2; \frac{1}{2}, 1, \frac{1}{2}, 1\right) \tag{45}$$

The Poisson flow becomes:

$$X_r^{\mathcal{E}}(t) := \Xi(0) - t^2\sum_{n=0}^{\infty} r^n\, e_n\, {}_4F_3\left(-n, n+2, \frac{1}{2}+\frac{it}{4}, \frac{1}{2}-\frac{it}{4}; \frac{3}{2}, 1, \frac{3}{2}; 1\right) \tag{46}$$

with:

$$e_n = \int_{0}^{\infty} \Phi(u)\, \tanh^{2n+2}(u)\,\mathrm{d}u \tag{47}$$

or:

$$e_n = -\frac{4}{\pi^3}\,(n+1)\int_{0^+}^{\infty} \frac{\Xi(u) - \Xi(0)}{u^2}\, we\left(\frac{u}{4}\right){}_4F_3\left(-n, n+2, \frac{1}{2}+\frac{iu}{4}, \frac{1}{2}-\frac{iu}{4}; \frac{3}{2}, 1, \frac{3}{2}; 1\right)\mathrm{d}u \tag{48}$$

Note 1: We are now working with the Poisson flow of $\frac{\Xi(t)-\Xi(0)}{t^2}$ instead of the direct flow of $\Xi(t)$.

Note 2: All equations above have been verified numerically, however a more rigorous proof about the domain of convergence would be desired.

E-mail Address: ra.dwars@quicknet.nl

E-mail Address: kalpesh.muchhal@iitbombay.org